

## On the use of Lineal Energy Measurements to Estimate Linear Energy Transfer Spectra

David A. Adams<sup>a</sup>, Leonard W. Howell, Jr.<sup>b</sup>, and James H. Adams, Jr.<sup>b,1</sup><sup>a</sup> Department of Physics, Virginia Polytechnic Institute and State University, Blacksburg, VA 24060; <sup>b</sup> Mail Code VP62, NASA Marshall Space Flight Center, Huntsville, AL 35812, USA

## ABSTRACT

This paper examines the error resulting from using a lineal energy spectrum to represent a linear energy transfer spectrum for applications in the space radiation environment. Lineal energy and linear energy transfer spectra are compared in three diverse but typical space radiation environments. Different detector geometries are also studied to determine how they affect the error. LET spectra are typically used to compute dose equivalent for radiation hazard estimation and single event effect rates to estimate radiation effects on electronics. The errors in the estimations of dose equivalent and single event rates that result from substituting lineal energy spectra for linear energy spectra are examined. It is found that this substitution has little effect on dose equivalent estimates in interplanetary quiet-time environment regardless of detector shape. The substitution has more of an effect when the environment is dominated by solar energetic particles or trapped radiation, but even then the errors are minor especially if a spherical detector is used. For single event estimation, the effect of the substitution can be large if the threshold for the single event effect is near where the linear energy spectrum drops suddenly. It is judged that single event rate estimates made from lineal energy spectra are unreliable and the use of lineal energy spectra for single event rate estimation should be avoided.

## INTRODUCTION

Linear Energy Transfer (LET) is the energy lost by an ionizing particle per unit pathlength traversed by the particle. The LET spectrum of ionizing particle radiation is used in radiation dosimetry to calculate the dose equivalent ( $I$ ) is given by

$$H = C \int_L Q(L) L f(L) dL, \quad (1)$$

where  $L$  is the LET,  $Q(L)$  is the Quality Factor and  $f(L)dL$  is the flux of ionizing particles having an LET between  $L$  and  $L + dL$ . The conversion factor,  $C = 4\pi t / \rho$ , is needed to get  $H$  in units of dose equivalent, where  $4\pi$  is the solid angle,  $t$  is time and  $\rho$  is the density of the tissue target. The LET spectrum is also used to estimate single event effect (SEE) rates in microelectronics (2, 20). The idealized formula for the SEE rate,  $N_e$ , is given by

---

<sup>1</sup> Mail Stop VP62, NSSTC, 320 Sparkman Drive, Huntsville, AL, 35805

$$N_e = 22.5\pi A Q_{crit} \int_{L_0}^{L_{max}} (1/L^2) d[p(L)] F(L) dL, \quad (2)$$

where  $A$  is the surface area of the SEE-sensitive junction in the electronic part,  $Q_{crit}$ , is minimum electrical charge required to produce an SEE. The pathlength required for an ion with LET,  $L$ , to deposit the charge,,  $Q_{crit}$ , in  $p(L) = 22.5/Q_{crit}/L$ . The lower bound of the integral is

$L_0 = 22.5Q_{crit}/p_{max}$ , where  $p_{max}$  is the largest diameter of the sensitive volume.  $d(p)$  is the probability density function for chord lengths across the sensitive junction and  $F(L) = \int_L f(L) dL$  is the integral LET spectrum. A more general expression for  $N_e$  has been presented by (21) that uses a Weibull function to describe the SEE cross section. Like equation (2), it has a threshold LET below which SEEs do not occur.

The LET spectrum is difficult to measure accurately because it must include the contributions from low energy ionizing particles that have very short ranges. A widely used instrument for measuring LET spectra is the tissue equivalent proportional counter (TEPC) (3).

The TEPC was developed for use in microdosimetry. It is designed to measure the energy deposited in a volume of tissue comparable in size to a cell or even a chromosome (4). A TEPC actually measures the lineal energy,  $y$  which is defined as the energy,  $\varepsilon$ , deposited in the sensitive volume of the TEPC divided by the mean chord length,  $\bar{l}$ , across that volume. The lineal energy spectrum is similar but not identical to the linear energy spectrum. Nevertheless the lineal energy spectrum is often been used as a measure of the LET spectrum (5,6,7) even though it is recognized that lineal energy is not an accurate measure of LET.

Lineal energy measurements made with TEPCs and similar single-element detectors differ from LET measurements in several ways (7, 8, 9). First of all, they do not measure the rate of energy loss per unit pathlength because the deposited energy,  $\varepsilon$ , is always divided by  $\bar{l}$  even though the distance over which the energy is lost is not fixed but varies from zero to the maximum diameter of the detector. Second, to measure the LET from very short range ionizing particles, it is necessary to use a very small detector volume. In addition, high energy particles will produce some delta rays with ranges that exceed the diameter of the detector's sensitive volume. If a sufficiently large fraction of the delta rays have such long ranges, the energy deposited by the high energy particle in the active volume of the detector will be significantly different from the energy lost. This is because the delta rays created within the sensitive volume will carry some of the energy outside. This loss will not be exactly compensated by the delta rays created outside the sensitive volume which deposit some of their energy in it (8).

Finally, delta rays created by high energy particles that are themselves not passing though the sensitive volume can enter it and deposit energy. This is especially important for the TEPC because of the difference in the density of the active detector (a gas) and the adjacent solid material. It has been shown both experimentally (8) and by simulations (10) that fast ions passing just inside the surface of the wall surrounding the TEPC's active volume can deposit up to twice the energy as high energy particles that traverse the full diameter of the sensitive volume. In this paper we will investigate the first of these causes by investigating the effect of using different shapes for the active

detector volume.

The shape of the detector's sensitive volume determines the distribution of chord lengths traversed by the ionizing particles passing through it. In addition to TPECs, which have been made with both spherical and cylindrical active volumes (11), various solid state microdosimeters have been proposed for measuring LET or lineal energy spectra (12, 13). Some of these use rectangular parallelepiped volumes. In this paper several sensitive volume shapes will be examined to determine how shape affects the correspondence between lineal energy spectra and LET spectra in typical space environments.

## COMPUTATIONAL METHODS

### *Ionizing Radiation Environments*

How the error due to substituting the lineal energy spectrum for the LET spectrum depends on the shape of the sensitive volume of the microdosimeter will be investigated for three space radiation environments:

- 1) the quiet time galactic cosmic ray (GCR) environment;
- 2) the solar energetic particle (SEP) environment during the events of October 1989 and
- 3) the trapped radiation (TR) environment at solar minimum in the orbit of the International Space Station.

These space radiation environments were calculated using an extended version of the CREME96 code (2). These extensions added to CREME96 allow the LET spectra to be calculated in water and allow the full LET spectra to be output, i.e., from minimum ionizing protons to stopping uranium.

*Galactic Cosmic Rays.* The LET spectrum is calculated in the Earth-Mars neighborhood of interplanetary medium. The calculation was done for the 1977 solar minimum.

*Solar Energetic Particles.* The SEP environment was computed in the interplanetary medium at 1 astronomical unit from the sun. The environment was for the worst day during the October, 1989 series of SEP events. The contribution from GCR environment was also included as it was in October, 1989.

*The Inner radiation Belt.* The environment averaged around the orbit of the International Space Station (ISS) was computed. The calculation was for solar minimum when the radiation belts are the most intense around this orbit. The GCR environment at solar minimum, modulated by the orbit-averaged geomagnetic cutoff transmission for the ISS orbit, was also included.

For all three environments the LET spectrum was calculated using the energy spectra of all the elements from hydrogen to uranium over the energy range from 0.1 MeV/nuc to 100,000 MeV/nuc. The calculation was done for the center of a spherical shell of aluminum with a wall thickness of 0.25 inches (0.635 g/cm<sup>2</sup>).

### *The Lineal Energy Spectra*

The lineal energy spectra that would be measured by a microdosimeter are computed assuming the signal,  $\varepsilon$ , is just the product of  $L$  and  $l$ , so  $y = Ll/\bar{l}$  where  $l$  is chord length traversed by the particle giving the signal,  $\varepsilon$ , and  $\bar{l}$  is the mean chord length. For convex surfaces, Cauchy (14) has shown that  $\bar{l} = 4V/S$ , where  $V$  is the sensitive volume and  $S$  is the area surrounding that volume. A recent review of the derivation of this formula has been published by Mazzolo, Roesslinger and

Grille (15).

The resulting differential lineal energy spectrum,  $\phi(y)$ , is given by

$$\phi(y) = \int_0^{l_{\max}} f\left[\frac{y(\bar{l}/l)}{\bar{l}}\right] d(l) \frac{\bar{l}}{l} dl \quad (3)$$

where  $f(L) = dF(L)/dL$ ,  $d(l)$  is the probability density of chord lengths and  $l_{\max}$  is the longest possible chord in the sensitive volume of the microdosimeter. To find out how well the lineal energy spectrum tracks the LET spectrum,  $f(L)$  and  $\phi(y)$  are compared.

#### *The Dose Equivalent*

The dose equivalent can be calculated using eq. (1) where the quality factor,  $Q$ , is defined in (1) as:

$$\begin{aligned} Q &= 1 & L &\leq 10 \text{KeV} / \mu\text{m} \\ Q &= 0.32L - 2.2 & 10 < L &\leq 100 \text{KeV} / \mu\text{m} \\ Q &= 300L^{-1/2} & L &> 100 \text{KeV} / \mu\text{m} \end{aligned}$$

To find out the effect of using the lineal energy spectrum instead of the LET spectrum to calculate the dose equivalent, we substitute  $\phi(y)$  and  $y$  for  $f(L)$  and  $L$  in eq. (1). With these substitutions made we obtain,

$$H' = C \int_0^{y_{\max}} Q(y) y \phi(y) dy \quad (4)$$

To find out the effect of this assumption on the dose equivalent,  $H'$  and  $H$  are compared.

#### *SEE Rate*

Similarly to find out the effect of using the lineal energy spectrum instead of the LET spectrum to calculate SEE rates, we substitute  $\Phi(y) = \int_y \phi(y) dy$  and  $y$  for  $F(L)$  and  $L$  in eq. (2) to obtain,

$$N'_e = 22.5\pi A Q_{\text{crit}} \int_{y_0}^{y_{\max}} (1/y^2) d[p(y)] \Phi(y) dy \quad (5)$$

#### *Chord Length Distributions*

We consider three shapes for the sensitive volume of microdosimeters: spheres, right circular cylinders and rectangular parallelepipeds. In this section we describe how the cord length probability density functions,  $d(l)$ , are calculated for each case. This calculation assumes an isotropic distribution of incident rays.

*The Sphere.* The probability density function for chord lengths in a spherical sensitive volume is

$$d(l) = 2l / l_{\max}^2 \quad (6)$$

where  $l_{\max}$  is the diameter of the sphere (18).

*The Rectangular Parallelopiped.* The probability density function for chord lengths in a sensitive volume having the shape of a rectangular parallelopiped was first derived in 1980 by M. D. Petroff. His derivation was included as an appendix by Pickel and Blandford (16). This derivation was simplified in 1984 by Bendel<sup>2</sup>. Since Bendel's report is not available in the open literature, his results are presented here. The probability density function  $d(l)$  is given by

$$d(l) = (g(l, a, b, c) + g(l, b, a, c) + g(l, a, c, b) + g(l, b, c, a) + g(l, c, b, a) + g(l, c, a, b)) / (\alpha\pi) \quad (7)$$

where  $a$ ,  $b$  and  $c$  are the length, width and height respectively,  $\alpha = 3(ab + ac + bc)$  and the function  $g$  is defined as:

$$g(l; u, v, w) = \frac{8v^2w}{u^2 + v^2} - l \left[ \frac{3uv}{l_{\max}t} \right]^2 \quad 0 \leq l < w,$$

$$g(l; u, v, w) = \left[ \frac{9v^2l}{u^2 + v^2} \right] - \left[ \frac{9lu^2v^2}{l_{\max}^2t^2} \right] - (u/l)\sqrt{l^2 - w^2} (8 + 4w^2/l^2) \\ + (12uvw^2/l^3) \tan^{-1}(v/u) - \left[ \frac{v^2w^4}{l^3(u^2 + v^2)} \right] \quad w \leq l < t$$

$$\text{and } g(l; u, v, w) = - \left[ \frac{9lu^2w^2}{l_{\max}^2(u^2 + v^2)} \right] + \frac{u^2w^2}{l^3} \left[ \frac{w^2}{u^2 + v^2} - 3 \right] + (12uvw^2/l^3) \tan^{-1}(v/u) \\ + (v/l)\sqrt{l^2 - u^2 - w^2} \left[ 4 + \frac{2t^2}{l^2} \right] - (12uvw^2/l^3) \cos^{-1} \left[ \frac{u}{\sqrt{l^2 - w^2}} \right] \quad t \leq l < l_{\max}$$

$$\text{where } l_{\max} = \sqrt{u^2 + v^2 + w^2} \quad \text{and} \quad t = \sqrt{u^2 + w^2}$$

*Comparison with Simulation.* Monte Carlo methods developed by Howell (19) are used to simulate the isotropically distributed trajectories by generating random chords within a sphere. A rectangular parallelopiped with the relative dimensions of 2:4:6 is placed in the containment sphere and the entry and exist points of those randomly distributed chords that intersect the parallelopiped are determined and hence, their chord lengths through the parallelopiped are calculated. A relative frequency histogram the cord lengths of one million simulated trajectories though the parallelopiped is shown in Fig. 1 along with the theoretical probability density function  $d(l; 2, 4, 6)$  obtained from eq. (7). This comparison shows excellent agreement between simulation and theory.

<sup>2</sup> W. L. Bendel, "Length Distribution of Chords Through a Rectangular Volume", NRL Memorandum Report, 1984

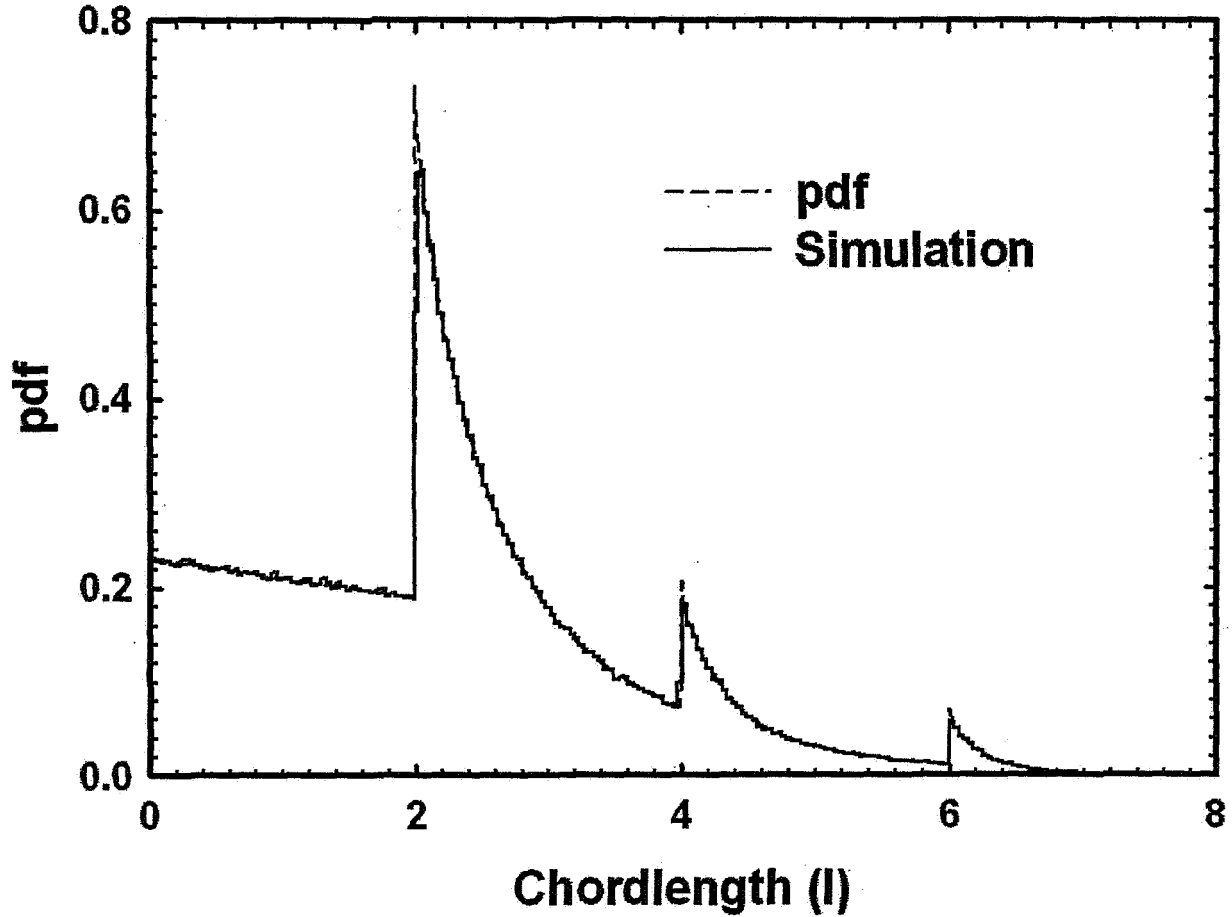


Fig. 1. Comparison of the theoretical and simulated chord length distributions for a rectangular parallelepiped with relative dimensions of 2:4:6. The simulation of the probability density function (pdf) is based on  $10^6$  simulated random cords.

*The Right Circular Cylinder.* The probability density function for chord lengths in a sensitive volume having the shape of a right circular cylinder was first derived by Mäder (17) and Kellerer (18) and recently simplified by Mäder (private communication). The results have been verified with simulations using the stochastic method of Howell (19). Letting  $D$  denote the diameter of the cylinder and  $H$  its height, the probability density function  $d(l)$  for chord length  $l$  is defined in terms of the probability density function of the random variable  $m = l/D$  (chord length relative to diameter) and the parameter  $e = H/D$  (elongation) having probability density function

$$c(m; e) = \frac{4}{\pi(e+1/2)} \left( e i_1(m, e) - m^2 i_2(m, e) + 2i_3(m, e) + \frac{e^2}{m^2} i_4(m, e) \right), \quad 0 \leq m \leq \sqrt{1+e^2}$$

as  $d(l; D, H) = \frac{1}{D} c(l/D, H/D)$ ,  $0 \leq l \leq \sqrt{D^2 + H^2}$ . (8)

The terms of  $c(m; e)$  are:

$$i_1(m, e) = \begin{cases} 3\pi/16, & m = 0 \\ \infty & m = 1 \\ \frac{1}{3m^4} \left( m^2 x \sqrt{(1-m^2x^2)(1-x^2)} - 2(1+m^2)E_1(x, m) + (2+m^2)F_1(x, m) \right) \Big|_{x=a(m, e)}^{x=b(m)} & m > 1 \end{cases}$$

where the evaluation limits  $b(m)$  and  $a(m, e)$  are:

$$b(m) = \begin{cases} 1, & m \leq 1 \\ 1/m, & m > 1 \end{cases} \quad \text{and} \quad a(m, e) = \begin{cases} 0, & m \leq e \\ \sqrt{1 - \frac{e^2}{m^2}}, & m > e \end{cases}$$

and

$$E_1(x, m) = \begin{cases} E(\sin^{-1} x, m^2), & m < 1 \\ mE(\sin^{-1}(mx), 1/m^2) - \frac{(m^2 - 1)F(\sin^{-1}(mx), 1/m^2)}{m}, & m \geq 1 \end{cases}$$

and

$$F_1(x, m) = \begin{cases} F(\sin^{-1} x, m^2), & m < 1 \\ \frac{F(\sin^{-1}(mx), 1/m^2)}{m}, & m \geq 1 \end{cases}$$

where  $F$  and  $E$  are the incomplete elliptic integrals  $F(\alpha, k) = \int_0^\alpha \frac{d\theta}{\sqrt{1 - k \sin^2 \theta}}$  and

$E(\alpha, k) = \int_0^\alpha \sqrt{1 - k \sin^2 \theta} d\theta$  of the first and second kind, respectively. Next,

$$i_2(m, e) = \begin{cases} 1/5, & m = 0 \\ \frac{1}{8m^5} \left( -mx \sqrt{1 - m^2 x^2} (3 + 2m^2 x^2) + 3 \sin^{-1}(mx) \right) \Big|_{x=a(m, e)}^{x=b(m)}, & m > 0 \end{cases}$$

and

$$i_3(m, e) = \begin{cases} 1/3, & m = 0 \\ \frac{1}{8m^3} \left( mx\sqrt{1-m^2x^2} (2m^2x^2 - 1) + \sin^{-1}(mx) \right) \Big|_{x=a(m,e)}^{x=b(m)}, & m > 0 \end{cases}$$

and

$$i_4(m, e) = \begin{cases} 0, & m \leq e \\ \frac{1}{2} \left( \cos^{-1}(\sqrt{m^2 - e^2}) - \sqrt{(m^2 - e^2)(1 - (m^2 - e^2))} \right), & m > e \end{cases}$$

*Comparison with Simulation.* Monte Carlo methods are used once again to simulate random chords in a sphere. A right circular cylinder of diameter  $D=1$  and height  $H=1.5$  is placed within the containment sphere and the randomly distributed chords within the cylinder are determined. A relative frequency histogram of these chord lengths is shown in Fig. 2 along with the theoretical probability density function  $d(l;1,1.5)$  given by eq. 6. This comparison shows excellent agreement between simulation and theory.

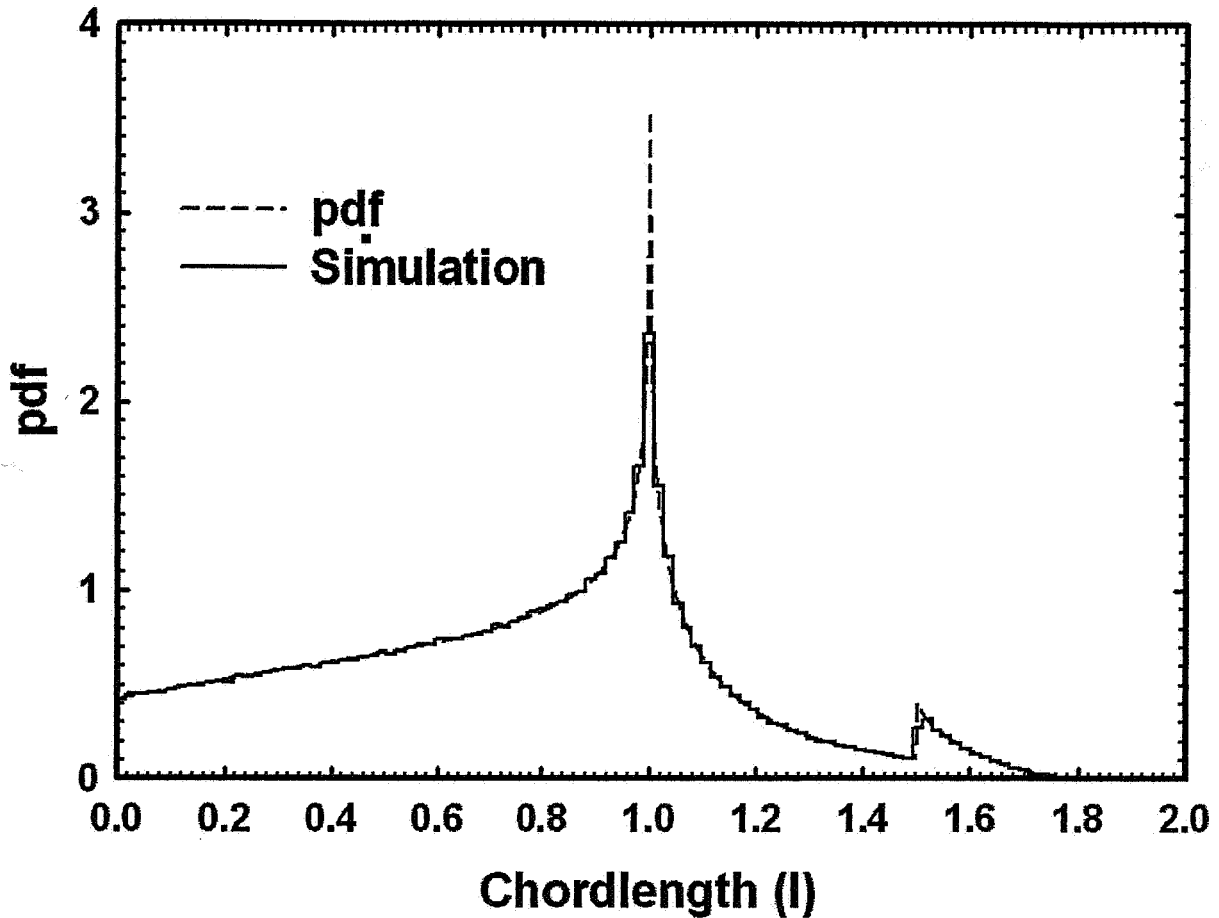


Fig. 2. Relative frequency histogram of one million simulated chord lengths in a cylinder of diameter 1 and height 1.5, along with the theoretical probability density function using eq. 6.

## RESULTS

### *LET Spectra*

The differential LET spectrum in the GCR behind  $0.635 \text{ g/cm}^2$  of aluminum in the local interplanetary medium is shown in Fig. 3. The lowest LET from any particle in the environment is  $0.198 \text{ KeV}/\mu\text{m}$ . This is the LET of minimum ionizing protons which occurs at about 2.9 GeV. This corresponds to the spike at the left of the curve.

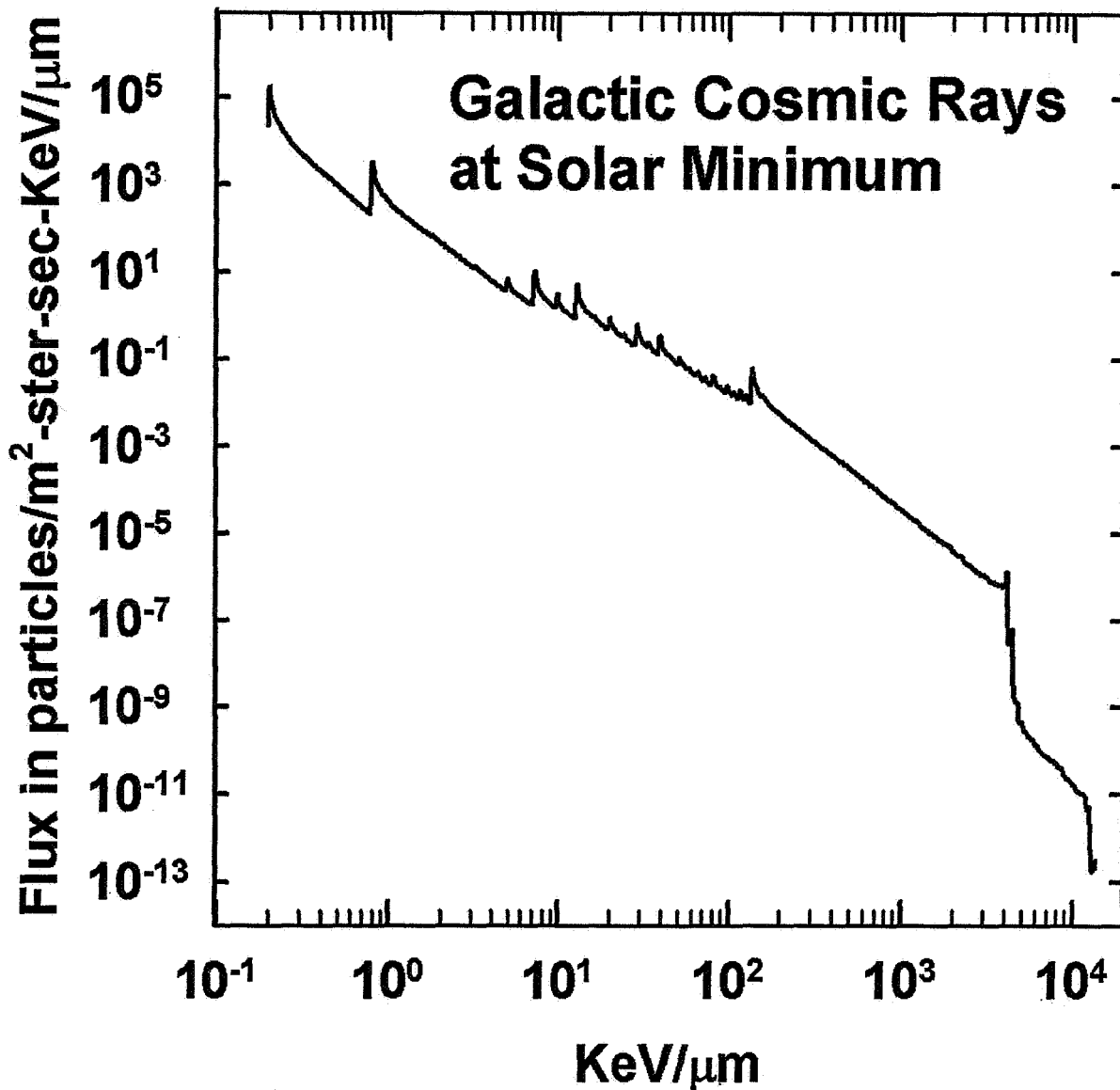


Figure 3. The differential GCR LET spectrum behind  $0.635 \text{ g/cm}^2$  of aluminum in the interplanetary medium during the 1977 solar minimum

The spectrum to the right of this point is due to protons at energies both below and above 2.9 GeV, where the LET is higher. To the right of the proton spike, there is another spike due to minimum ionizing helium. Farther to the right additional peaks can be seen that are due to the minimum ionizing nuclei of the more abundant elements, B, C, N, O, etc. The spectrum extends to the LET of stopping Th and U in the lower right corner.

Fig. 4 shows the average differential LET spectrum for the day of 20 October, 1989. On this day the largest SEP event of the October 1989 series was observed at 1 AU. Solar energetic protons dominate the LET spectrum from  $0.198 \text{ KeV}/\mu\text{m}$  up to the Bragg peak for protons at  $\sim 100 \text{ KeV}/\mu\text{m}$ , which is due to protons with energies of  $\sim 85 \text{ KeV}$ . The flux at higher LET values is due to heavier elements in the SEP event. The Bragg peak due to Helium nuclei at  $\sim 180 \text{ KeV}/\text{nuc}$  can be seen at  $\sim 200 \text{ KeV}/\mu\text{m}$ . The peaks at higher LET values are due to relativistic nuclei heavier than Fe. While these relativistic nuclei come primarily from the GCRs, the nuclei heavier than Fe at lower energies

are primarily from the SPE.

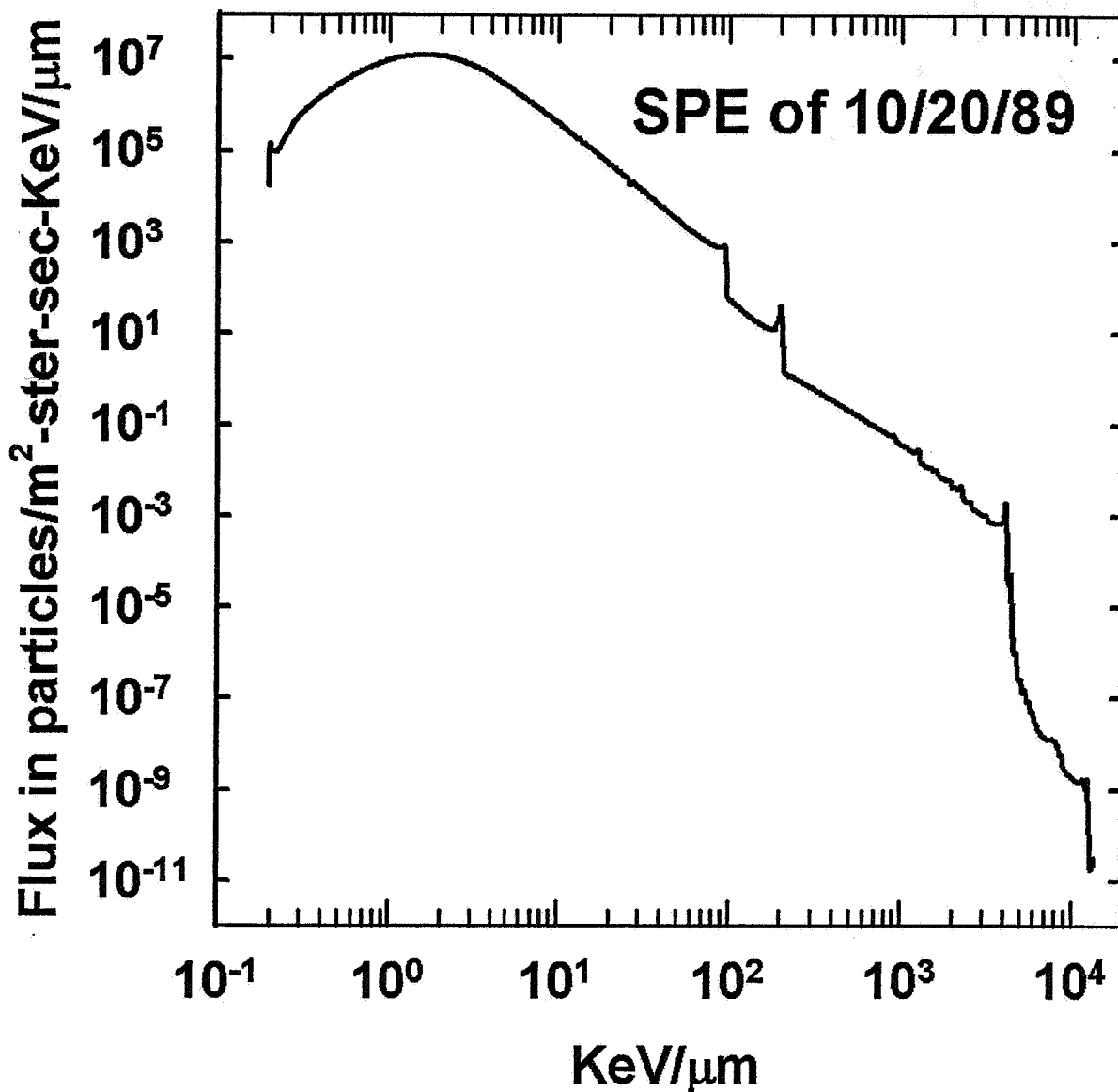


Figure 4: The differential LET spectrum in interplanetary space near earth during the worst day of the October, 1989 SEP event behind 0.635 g/cm<sup>2</sup> of aluminum.

The LET spectrum averaged around the orbit of the International Space Station (ISS) is shown in Fig. 5. Like the LET spectrum during a SEP event shown in Fig. 4, the spectrum at LET values below ~100 KeV/μm, except for the peak at 0.198 KeV/μm, is due to protons trapped in the inner radiation belt. This peak is due to minimum-ionizing GCR protons. Unlike the case in figure 4, this peak can be seen above the orbit-averaged trapped protons because they are not as intense as the SPEs. Also unlike the SEP environment, ions heavier than protons are virtually absent from the TR so the peaks due to relativistic GCRs dominate the LET spectrum to the right of the proton Bragg peak at ~100 KeV/μm. The GCR spectrum for the ISS orbit is modulated by the orbit-averaged geomagnetic cutoff for the ISS orbit so the lower energy part of the GCR spectrum is attenuated.

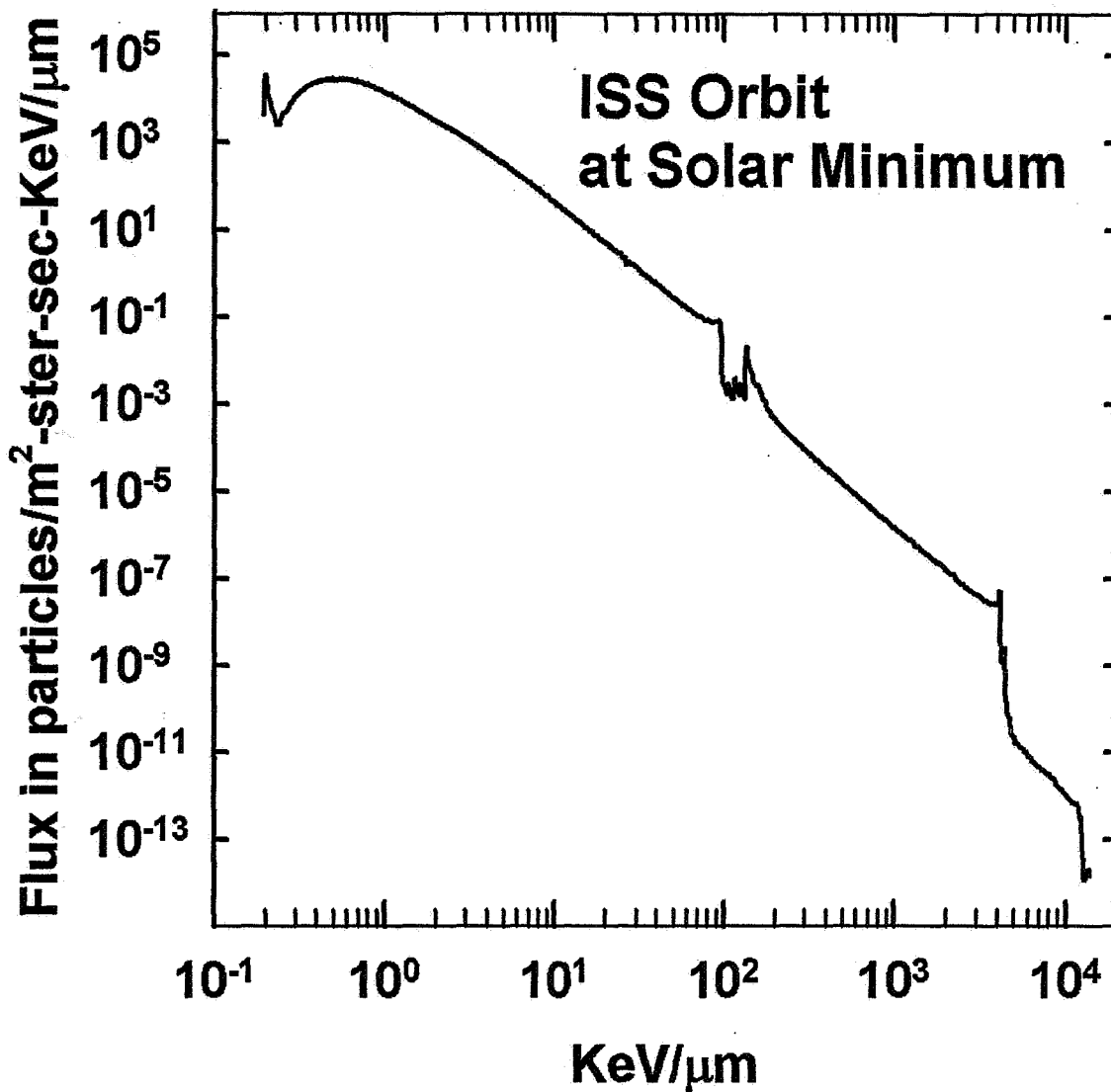


Figure 5. The average LET spectrum in the orbit of the International Space Station behind 0.635 g/cm<sup>2</sup> of aluminum in quiet times during the 1977 solar minimum.

#### *Comparison of LET Spectra and Lineal Energy Spectra*

In this section we will compare the differential LET spectra shown in Figs. 3, 4 and 5 with the lineal energy spectra that would be measured in the same environments using sensitive volumes of different shapes. These calculations are done using equation (3). Figure 6 compares the GCR LET spectrum shown in Fig. 3 with the lineal energy spectrum that would be measured using a small spherical sensitive volume in the same environment. The lineal energy spectrum differs considerably from the linear energy spectrum. First of all, it extends to non-physically small values of LET. This is because the real trajectory of a particle in the detector and therefore the signal recorded by the detector extend down to zero. To obtain the lineal energy, the signal is always divided by the mean chord length so the lineal energy spectrum also extends down to non-physically small values of LET. In principle, this is true of all single-detector lineal energy measuring devices. In the region where the two spectra overlap, the lineal energy spectrum is in disagreement with the LET spectrum near all its

sharp features and in a small range near  $3 \times 10^3$  KeV/ $\mu\text{m}$  where the LET spectrum declines sharply. These differences occur because cosmic rays traversing chords in the spherical detector that exceed the mean chord length yield lineal energy measurements that are higher than the LET of the cosmic rays producing them.

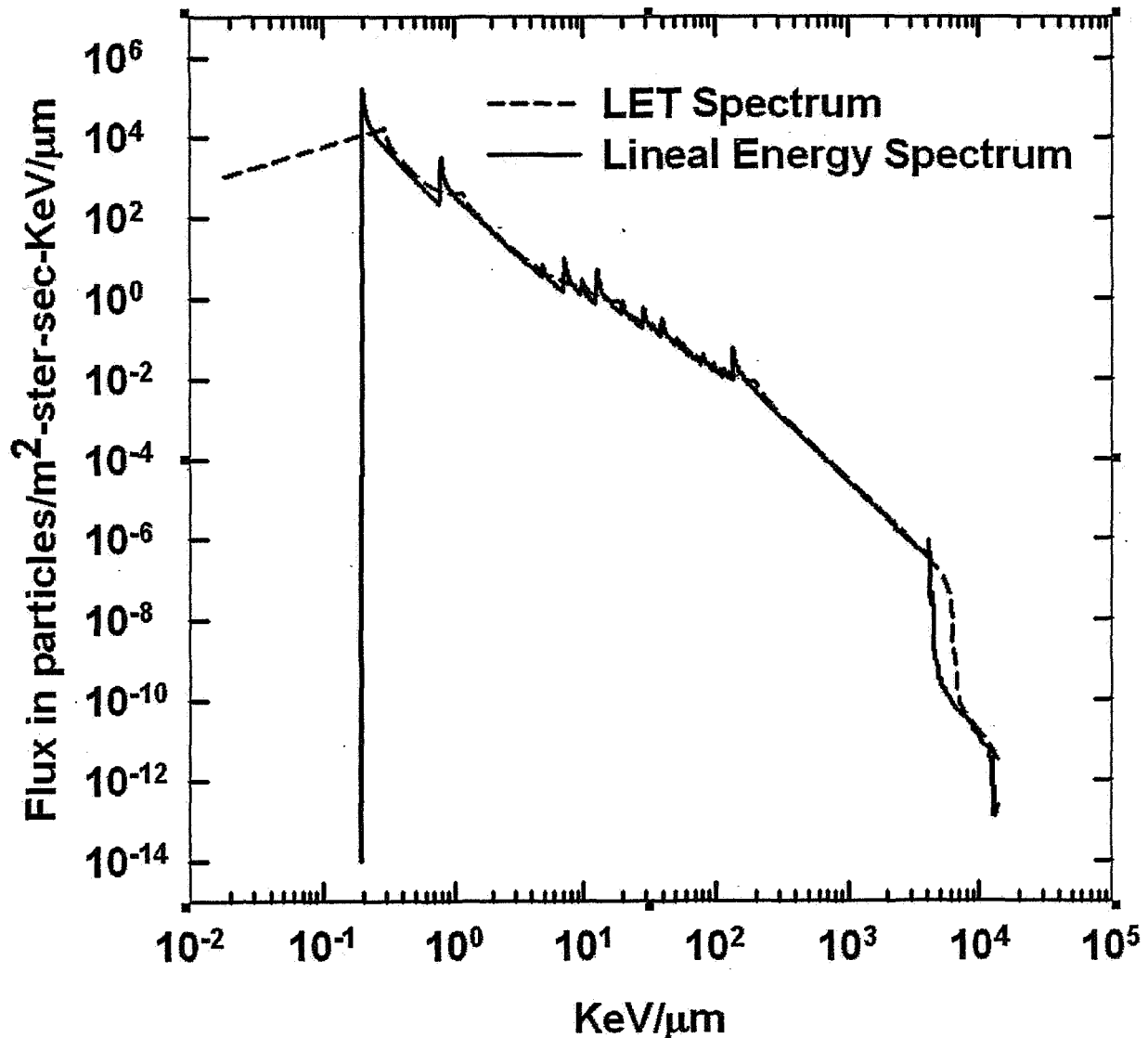


Figure 6. Comparison of the LET spectrum (solid black curve) in the GCR environment with the lineal energy spectrum (dashed red curve) measured in the same environment with a small spherical detector.

In Fig. 7 the same LET spectrum is compared with the lineal energy spectrum measured using a small cubical detector. In this and subsequent figures, we have suppressed the extension of the lineal energy spectrum to non-physically small values of LET. Where the two spectra overlap, the overall disagreement is somewhat worse than in the case of the sphere.

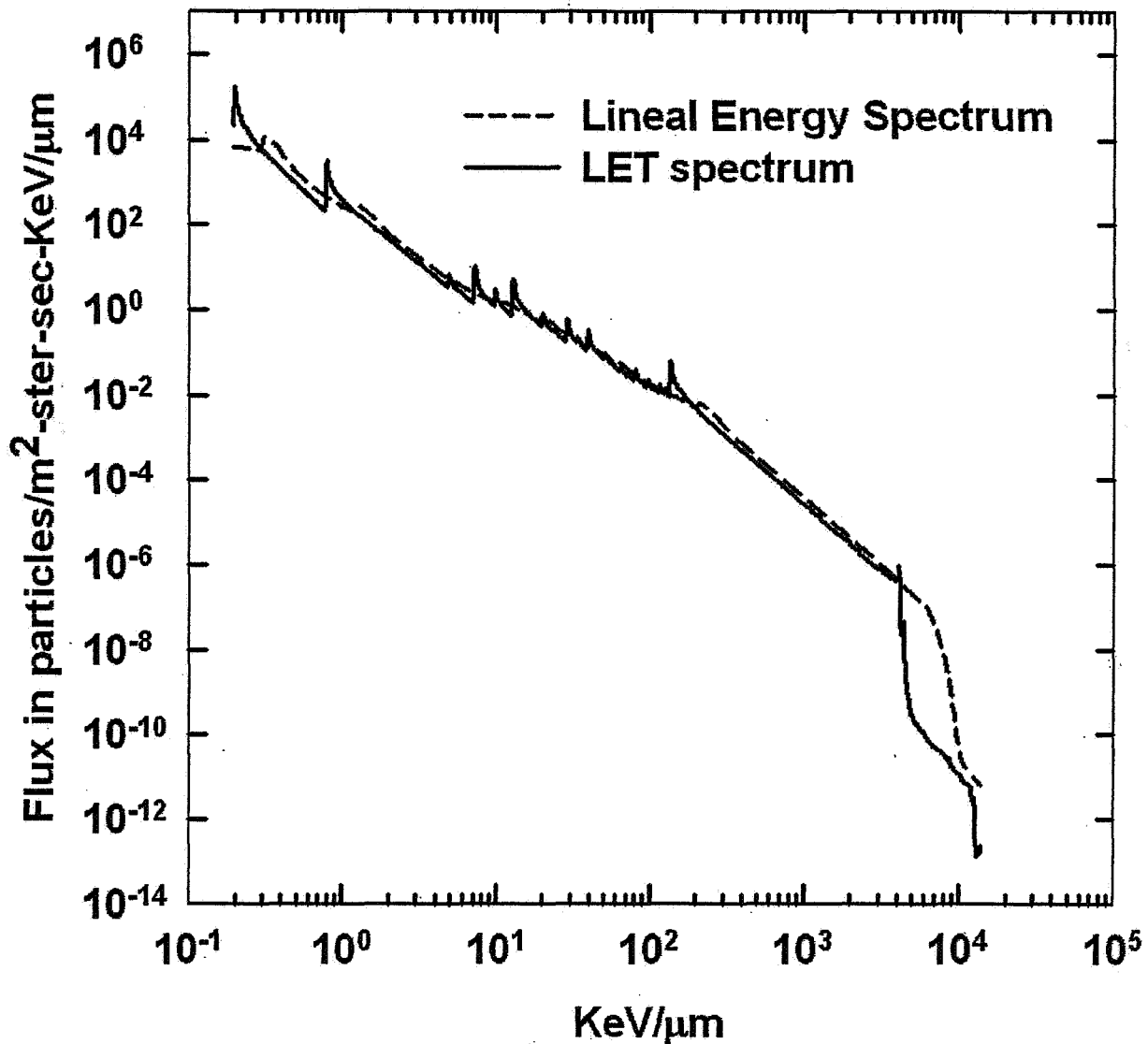


Figure 7. Comparison of the LET spectrum (solid black curve) in the GCR environment with the lineal energy spectrum (dashed red curve) measured in the same environment with a small cubical detector.

In Fig. 8 the same LET spectrum is once again compared with the lineal energy spectrum, this time measured using a small right circular cylindrical detector whose height and diameter are equal. Where the two spectra overlap, the only close agreement between them is between 300 and 2000 KeV/μm. Overall the disagreement looks comparable to the case of the cube.

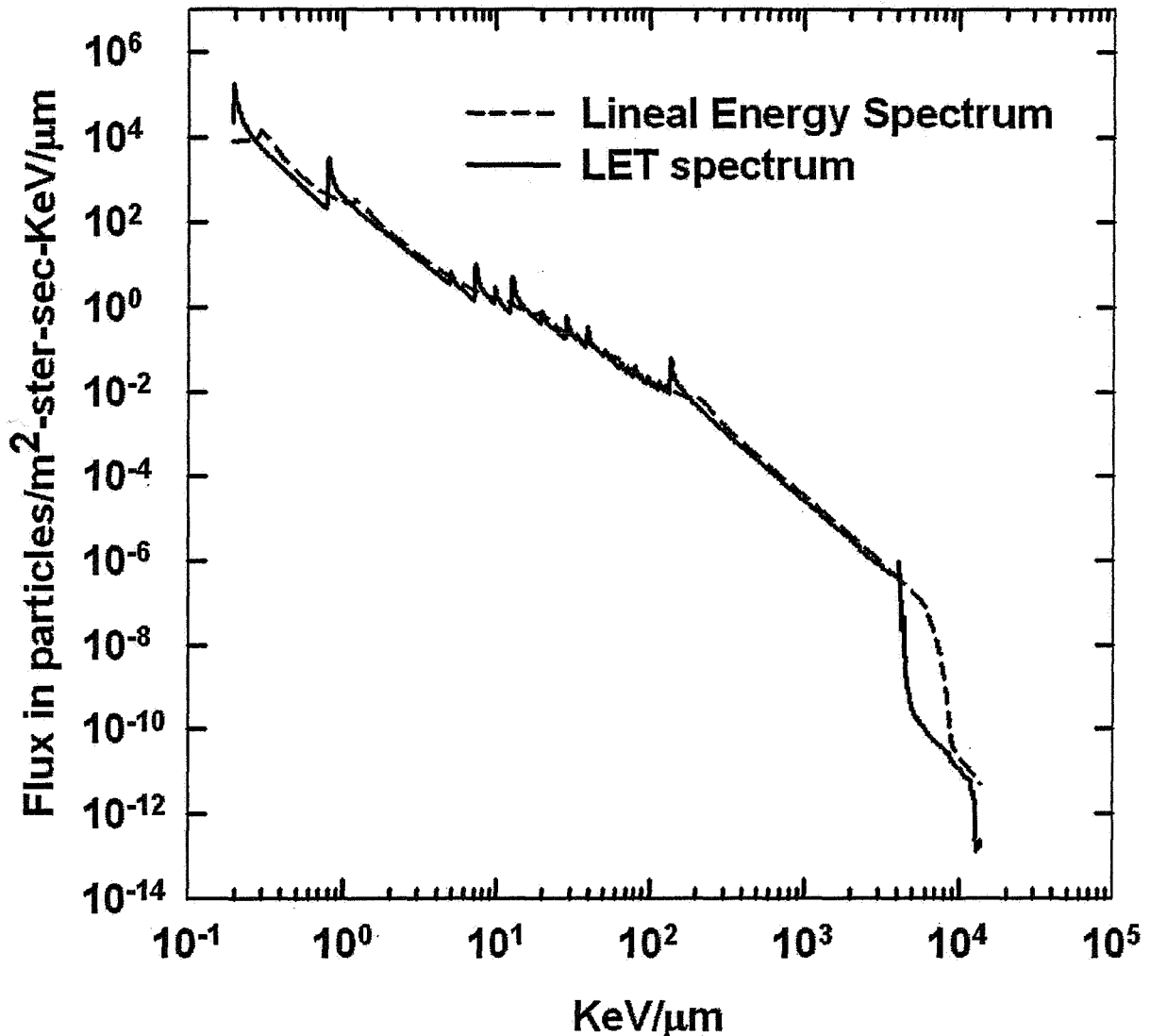


Figure 8. Comparison of the LET spectrum (solid black curve) in the GCR environment with the lineal energy spectrum (dashed red curve) measured in the same environment with a small right circular cylindrical detector whose height is equal to its diameter.

The GCR LET spectrum and the lineal energy spectra measured with detectors of all three shapes disagree strongly near the sharp features in the LET spectrum. Near these features the LET spectrum exceeds the lineal energy spectrum by as much as 1400%, 2000% and 2500% for measurements made using the spherical, cubical and cylindrical detectors, respectively. The lineal energy measurements overestimate the LET spectra between  $4 \times 10^3$  and  $1 \times 10^4$  KeV/ $\mu$ m for all three detector shapes.

Figures 9 and 10 compare lineal energy spectra for a spherical detector to the LET spectra for measurements made in the SPE and ISS environments shown in figures 4 and 5, respectively.

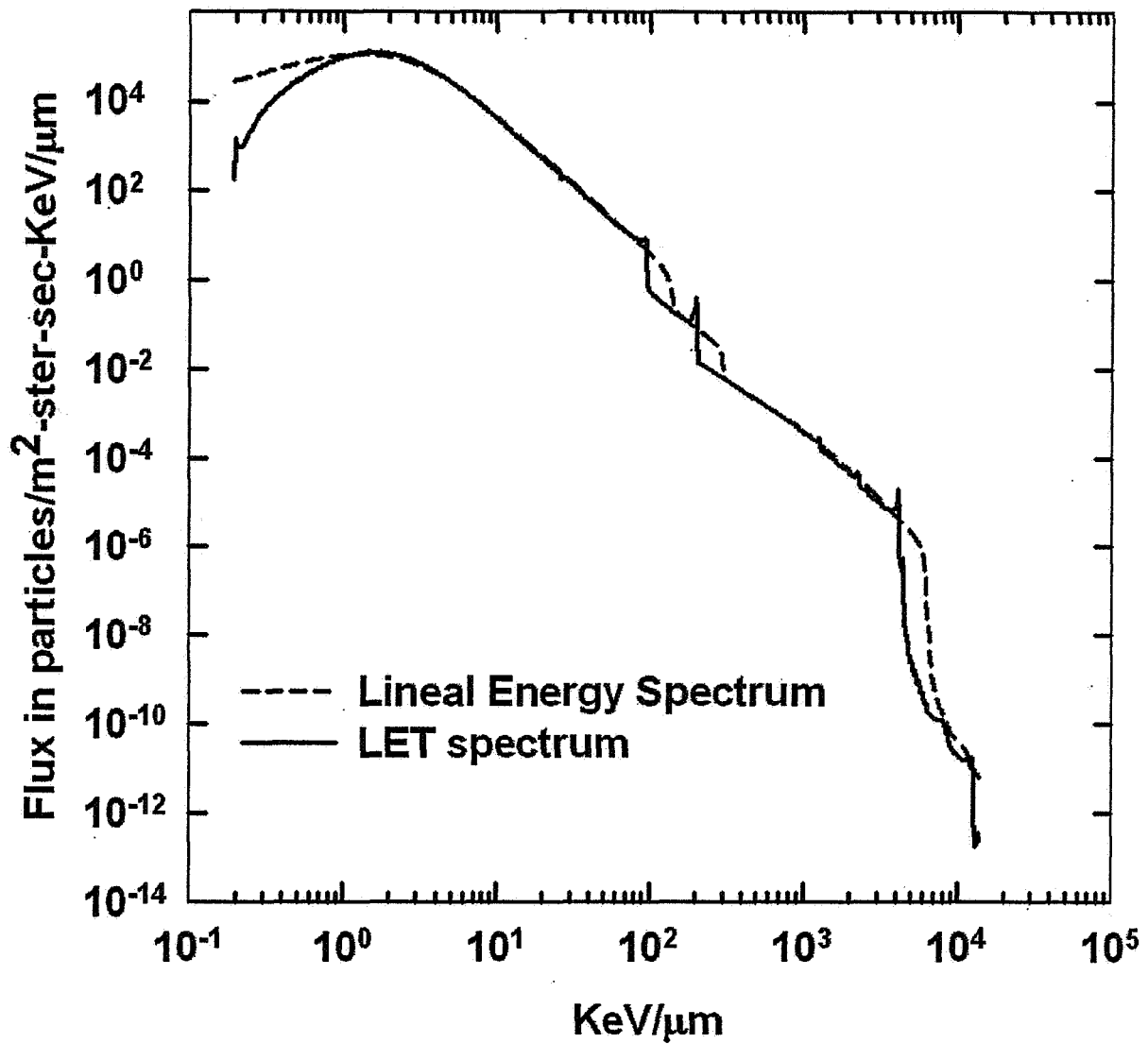


Figure 9. This figure compares the lineal energy spectrum for a spherical detector with the LET spectrum for the SPE environment shown in figure 4.

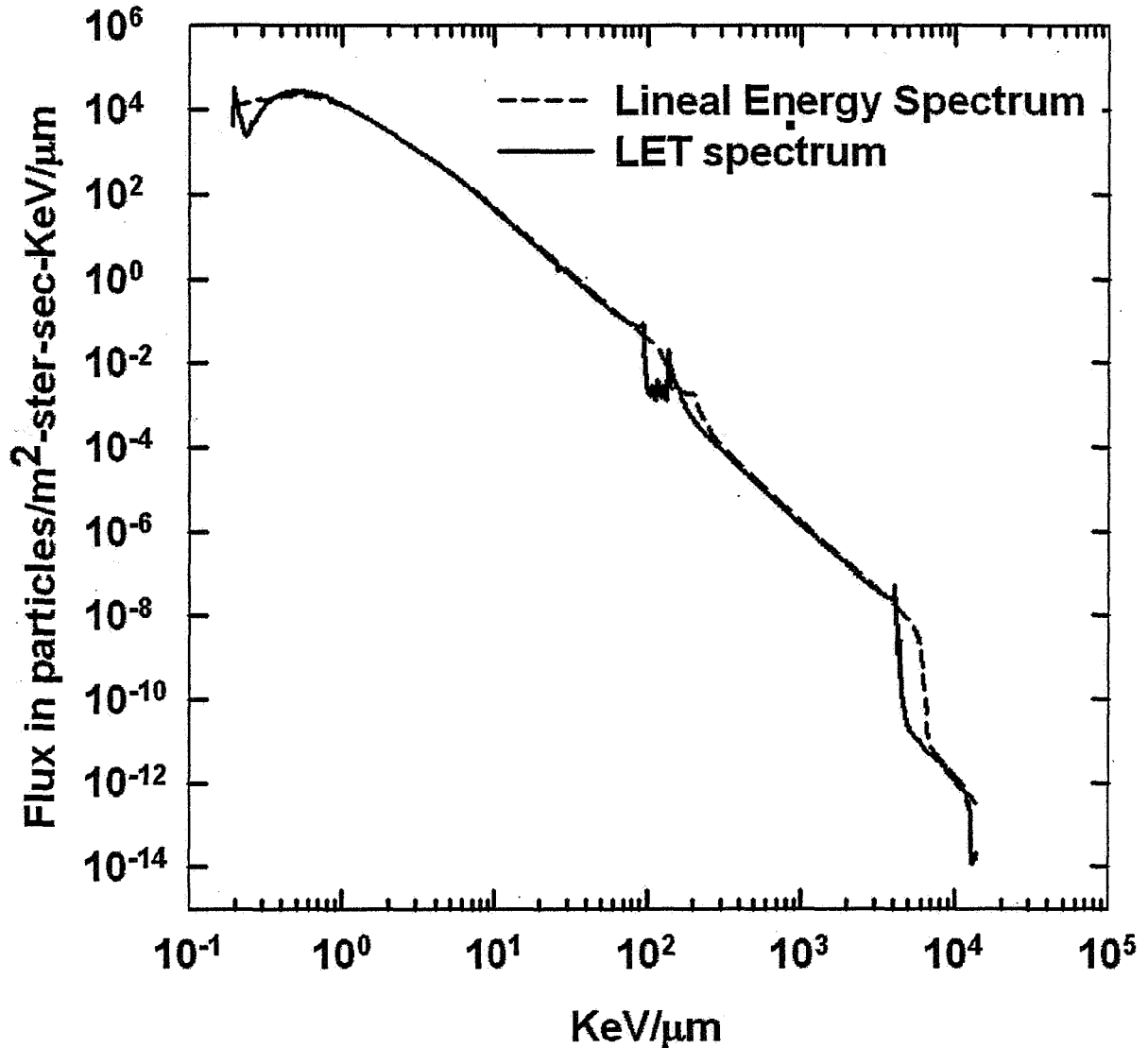


Figure 10. This figure compares the lineal energy spectrum for a spherical detector with the LET spectrum for the ISS environment shown in figure 5.

The discrepancies between the LET and lineal energy spectra are larger for the SPE and ISS environments. They are also worse when the detector shape is a cylinder with equal diameter and height and a bit worse still for a cubical detector.

#### *Dose Equivalent calculations*

Using equations (1) and (4), we compare the dose equivalent calculated using the LET spectra for the three environments to the lineal energy spectra from these environments for the cases of sphere, cylindrical, and rectangular parallelepiped detectors. The % difference between the true dose equivalent,  $H$ , and that computed by substituting a lineal energy spectrum,  $H'$  is given by  $100\% \times (H - H') / H$ . Table 1 shows the results for the three detector shapes in the three environments. The results show that the errors made by using lineal energy spectrum measurements

for the LET spectrum in the calculation of the dose equivalent are not very large for the environments and detector shapes considered.

Table 1

<u>Detector Shape</u>	<u>Error in %</u>		
	<u>GCR</u>	<u>ISS</u>	<u>SPE</u>
Sphere	-.65	6.3	11.
Cylinder	.51	13.	22.
Cube	1.1	17.	28.

The reason that the errors are so small despite the large discrepancies between the LET and linear energy spectra can be understood by remembering that both spectra measure the same flux of particles. The only difference is that the lineal energy spectrum smears the flux of particles with LET,  $L$ , to both lower and higher LET values near  $L$ . The dose equivalent is computed by integrating over the differential spectrum weighting the integrand with  $L$  (or  $y$ ) and  $Q(L)$  (or  $Q(y)$ ) which varies no faster than  $L$  (or  $y$ ). Because three shapes chosen smear the LET spectrum over  $\leq 2$  in  $L$  (or  $y$ ) as can be seen from the separation of the spectra where the LET spectrum falls steeply near  $3 \times 10^3$  KeV/ $\mu$ m in figures 6 through 10. This conclusion suggests that a detector shape having a maximum chord length much larger than the mean chord length would produce a larger discrepancy in the dose equivalent calculated in the two ways. To test this conclusion, a parallelepiped with a length and width ten times larger than its thickness was used for the detector volume. The result for the three environments was discrepancies of 0.33%, 32% and 47% for the GCR, ISS and SPE environments respectively. The results for the ISS and SPE environments are worse as expected. The result for the GCR environment is actually better than for the other shapes. This is presumably some compensation effect that results from smearing the LET spectrum between the relativistic particle peaks in the GCR LET spectrum.

*Single Event Effect Calculations*

LET spectra are also used to estimate SEE rates in microelectronic devices. In the idealized case where the device has a single sensitive volume whose size does not depend on LET, equations (2) and (5) can be used to estimate SEE rates from LET spectra and lineal energy spectra, respectively. This idealized method supplies accurate SEE rates for many devices.

These equations are based on the concept of an LET threshold,  $L_0$  (or  $y_0$ ). Unlike the computation of dose equivalent, the integrals do not extend over the entire spectra but begin from this threshold. With this in mind, examining the LET and lineal energy spectra in figures 6 through 10 reveals ranges of LET can be found where the differential flux drops suddenly. These regions can be found near  $5 \times 10^3$  KeV/ $\mu$ m and also near  $10^2$  KeV/ $\mu$ m in the ISS and SPE environments shown in figures 9 and 10. When the threshold is at the low LET side of one of these regions, we can expect SEE rate predictions that are significantly in error when the lineal energy spectrum is substituted for the LET spectrum. Table 2 gives some examples for the GCR environment.

Table 2

<u>LET Threshold</u> <u>In KeV/<math>\mu</math>m</u>	<u>Sphere</u> <u>% Error</u>	<u>Cube</u> <u>% Error</u>
5037	249	15400
3918	7280	46800
2800	369	838
1680	28	92
560	22	50
503	31	66
280	15	43

Table 2 shows that the error in the SEE rate depends strongly on the LET threshold for SEEs to occur. Since the lineal energy spectrum from the spherical detector is a more faithful representation of the LET spectrum, the errors in the SEE rate due to substituting the lineal energy spectrum measured with a spherical detector are smaller. The errors caused by substituting the lineal energy spectrum for the LET spectrum in the other two environments considered here are larger.

## DISCUSSION AND CONCLUSIONS

In this paper we have examined how lineal energy spectra differ from LET spectra depending on the environment and the shape of the device used to measure the lineal energy spectrum. We have found significant differences in some LET ranges that amount to hundreds of percent. These differences are smallest in the GCR environment in interplanetary space. In this environment they will be smallest for lineal energy measurements made with a spherical detector. A cylindrical detector with the height and diameter equal is slightly better than a cube and all shapes that produce broader path length probability density functions, such as the square rectangular parallelepiped with length and width ten times larger than its thickness examined here, give lineal energy spectra that smooth the spikes in the GCR LET spectrum and thus tend to conform more closely to it except beyond  $4 \times 10^3$  KeV/ $\mu$ m where the LET spectrum drops suddenly. Beyond this point, the lineal energy spectrum is running orders of magnitude above the LET spectrum.

We also examined the ISS environment and the SPE environment during a large SPE. Here also lineal energy spectra measured with the spherical detector conformed closest to the LET spectra, but not as close as in the GCR environment. Results obtained with the cylindrical detector conformed more closely than those from the cubical detector. All detectors produced lineal energy spectra that conformed more closely to the LET spectrum in the ISS environment than the SPE environment. The rectangular parallelepiped detector produced lineal energy spectra that conformed to the LET spectra worst for both the ISS and SPE environments.

### *Dose Equivalent Calculations*

We examined how well these lineal energy spectra performed when substituted for LET spectra in dose equivalent calculations. It was found that the dose equivalent calculated by substituting a lineal energy spectrum for an LET spectrum worked best in the GCR environment. Errors were  $\leq 1.1\%$  for all detector shapes tried. Errors were worse in the ISS and SPE environments. The spherical detector produced the least error, 6.3% and 11% respectively in the ISS and SPE environments.

Considering the other sources of error in estimating the health risks from space radiation, these errors are probably acceptable. Error using the other detector shapes in the ISS and SPE environments were worse, especially the parallelepiped shape. We can conclude that the best shape is spherical although a right circular cylinder with equal height and width produced acceptable results. For dose equivalent measurements in environments that differ significantly from the GCR environment, other shapes should be avoided.

#### *Single Event Effect Calculations*

The substitution of linear energy spectra for LET spectra in the computation of SEE rates can lead to large errors. This is especially true when the SEE threshold falls just below an LET value where the spectrum declines steeply. The lineal energy spectra conform poorly to the LET spectra in these regions regardless of the detector shape used. Because of the potentially large errors that can result, computation of SEE rates using lineal energy spectrum measurements should be avoided.

#### *Other Factors Affecting Lineal Energy Spectra*

Finally some comments are due on the other factors affecting measured lineal energy spectra that were not investigated in this paper.

Slowing and stopping particles change their LET as they pass through the detector. This causes the higher LET delivered as the particle slows is missed because the measurement gives the average LET over the path of the particle through the detector. This effect can be minimized by using small detector volumes.

As mentioned in the introduction, wall effects can strongly affect lineal energy measurements in gas filled detectors. This is especially true when the environment is dominated by fast heavy ions as is the case in space. These fast particles also produce delta rays with ranges longer than most chord lengths through small detector volumes. In this case the energy lost by delta rays created in the detector that escape may not be compensated by delta rays created outside the detector volume but depositing energy in the detector.

The results presented here have assumed that the particle flux was isotropic. When this is not the case, the lineal energy spectra measured by detectors that are not spherical can be further distorted and therefore be in stronger disagreement with the LET spectrum.

As mentioned in the introduction, solid state microdosimeters offer an alternative to gas filled detectors like the tissue-equivalent proportional counter. In these semiconductor detectors, the sensitive volume is defined by the geometry of a diode junction that is reverse biased. This junction must be small (to measure the LET due to stopping particles) so it is usually impeded as a circuit feature in a silicon wafer. In this case, the charge collected on the junction will include charge that diffuses in from the surrounding silicon. This contribution from diffusion depends on the particle's trajectory and the presence of insulating substrates and/or walls in the device design. In addition, highly ionizing particles create so many hole-electron pairs that the presence of these charged particles affects the distribution of electric fields in and around the junction, dynamically altering its shape (21). The result is the funnel effect (22). In this case charge is efficiently collected from the particle's track outside the junction increasing  $\epsilon$  and thus  $y$ .

Technically, it is very challenging to measure the complete lineal energy spectrum, including the contributions from low energy particles because this requires the use of very small detector volumes with the attendant sources of error mentioned above. To the extent that the wall effects in gas-filled detectors and the effects due to high energy delta rays can be modeled correctly, they can be

deconvolved from the lineal energy spectra. It is also possible to model diffusion and the funnel effect caused by heavy ions in solid state microdosimeters (23) but this is very computationally intensive. Further work is needed to develop the required understanding of these effects so that deconvolution techniques can be developed to recover the lineal energy spectra from micro-volume detectors in semiconductor devices.

### ACKNOWLEDGMENTS

The authors would like to thank Dr. U. Maeder for extensive consultations on the problem of the chord length probability density function for right circular cylinders. This work was supported in part by the Radiation Hardened Electronics for Space Environments Project at NASA Marshall Space Flight Center.

### REFERENCES

1. International Commission on Radiation Units and Measurements, *Conversion Coefficients for use in Radiological Protection Against External Radiation*. ICRU Report 57, ICRU Publications, Bethesda, MD, 1998.
2. A. J. Tylka, James H. Adams, Jr., Paul R. Boberg, Buddy Brownstein, William F. Dietrich, Erwin O. Flueckiger, Edward L. Petersen, Margaret A. Shea, Don F. Smart, and Edward C. Smith, CREME96: A Revision of the Cosmic Ray Effects on Micro-Electronics Code. *IEEE Trans. on Nucl. Sci.*, **44**, 2150-2160 (1997).
3. H. H. Rossi, H.H. and W. Rosenzweig, A device for the measurement of dose as a function of specific ionization. *Radiology*, **64**, 404-411 (1955).
4. P. Kliauga, Measurement of Single Event Energy Deposition Spectra at 5 nm to 250 nm Simulated Site Sizes. *Radiat. Prot. Dosim.*, **31**, 119-124 (1990).
5. Gautam Badhwar, Radiation Measurements on the International Space Station. 11<sup>th</sup> Annual NASA Space Radiation Health Investigators' Workshop, Arona (Italy), 287-291 (2000).
6. Tadayoshi Doke, Takayoshi Hayashi, and Thomas B. Borak, Comparisons of LET Distributions Measured in Low Earth Orbit Using Tissue Equivalent Proportional Counters and the Position-Sensitive Silicon-Detector Telescope (RRMD-III). *Radiat. Res.*, **156**, 310-316, (2001)
7. B. B. Gersey, T. B. Borak, S. B. Guetersloh, C. Zeitlin, J. Miller, L. Heilbronn, T. Murakami, and Y. Iwata, The Response of a Spherical Tissue-Equivalent Proportional Counter to Iron Particles from 200-1000 MeV/nucleon. *Radiat. Res.*, **157**, 350-360 (2002).
8. Stephen Guetersloth, Thomas B. Borak, Phillip J. Taddei, Cary Zeitlin, Lawrence Heilbronn, Jack Miller, Takeshi Murakami, and Yoshiyuki Iwata, The Response of a Spherical Tissue-Equivalent Proportional Counter to Different Ions Having Similar Linear Energy Transfer. *Radiat. Res.*, **161**, 64-71 (2004)
9. S. E. Rademacher, T. B. Borak, C. Zeitlin, L. Heilbronn and J. Miller, Wall Effects Observed in Tissue-Equivalent Proportional Counters from 1.05 GeV/nucleon Iron-56 Particles. *Radiat. Res.*, **149**, 387-395 (1998).
10. H. Nikjoo, I. K. Khvostunov and F. A Cucinotta, The response of tissue equivalent proportional counters to heavy ions. *Radiat. Res.*, **157**, 435-445 (2002).
11. Jay Burmeister, Chandrasekhar Kota, Richard L Maughan and Anthony J. Waker, Characterization of miniature tissue-equivalent proportional counters for neutron radiotherapy applications. *Phys. Med. Biol.*, **47**, 1633-1645 (2002).
12. D. R. Roth, P. J. McNulty, W. J. Beauvais, R. A. Reed and E. G. Stassinopoulos, Solid State

- Microdosimeter for Radiation Monitoring in Spacecraft and Avionics. *IEEE Trans. on Nucl. Sci.*, **41**, 2118 (1994).
13. P.D. Bradley, A.B. Rosenfeld, K.K.Lee, D.N. Jamieson, G. Heiser, and S. Satoh, Charge Collection and Radiation Hardness of a SO1 Microdosimeter for Medical and Space Applications. *IEEE Trans. on Nucl. Sci.*, **45**, 2700-2710 (1998).
  14. A. Cauchy, Memoire sur la rectification des courbes et la quadrature des sourface courbe. *Oeuvres Completes*, 2 (Gauthier-Villard, Paris) (1908).
  15. Alain Mazzolo, Benoit Rosslinger and Wilfried Grille, Properties of chord length distributions of nonconvex bodies. *J. Math. Phys.*, **44**, 6195-6208 (2003).
  16. J. C. Pickel and J. T. Blanford, Jr., Cosmic-Ray-Induced Errors in MOS devices, *IEEE Trans. on Nucl. Sci.*, **NS-27**, 1006-15 (1980) . Erratum, *ibid.* **NS-29**, 2122 (1982).
  17. U. Mäder, Chord Length Distributions for Circular Cylinders. *Radiat. Res.*, **82**, 454-466 (1980).
  18. Albrecht M. Kellerer, Conditions on the Random Traversal of Convex Bodies and Solutions for General Cylinders. *Radiat. Res.*, **47**, 359-376 (1971).
  19. Leonard W. Howell, Jr., A Stochastic Model for Particle Impingements on Orbiting Spacecraft. *J. Astron. Sci.*, **34**, 375-401 (1986).
  20. James H. Adams, Jr. The Variability of Single Event Upset Rates in the Natural Environment. *IEEE Trans. on Nucl. Sci.*, **NS-30**, 4475-4480 (1983).
  21. Peter D. Bradley. The Development of a Novel Silicon Microdosimeter for High LET Radiation Therapy. 1-333. Ph.D. Thesis, Department of Engineering Physics, University of Wollongong (2000).
  22. E.L. Petersen, J.C. Pickel, J.H. Adams, Jr., and E.C. Smith, Rate Prediction for Single Event Effects - a Critique. *IEEE Trans. on Nucl. Sci.* **NS-39**, 1577-1599 (1992).
  23. Paul E. Dodd. Physics-Based Simulation of Single-Event Effects. *IEEE Trans. on Mat. Rel.* **5**, 343-357 (1992).